JOURNAL OF GUIDANCE, CONTROL, AND DYNAMICS
Vol. 25, No. 6, November–December 2002

Spherical μ with Application to Flight Control Analysis

Shinji Ishimoto* and Fuyuto Terui†
National Aerospace Laboratory, Tokyo 182-8522, Japan

Robust stability analysis problems for linear systems subject to real parametric uncertainties are treated. We assume that uncertainties are restricted to a hypersphere in a parameter space. This constraint is represented by an inequality with respect to the Euclidean norm of a parameter vector. From a statistical point of view, the use of a spherical constraint can be justified if uncertain parameters are Gaussian-distributed random variables. We define an extended version of the real structured singular value, which is referred to as spherical (real) μ, for a spherical uncertainty set. Geometrically, the reciprocal of spherical μ means the radius of a guaranteed stable spherical region. We newly develop an upper bound of spherical μ, which is similar to a well-known upper bound of standard μ for a cubical uncertainty set, that is, parametric uncertainties subject to interval constraints. As its counterpart, the spherical μ upper bound can be computed by solving a linear matrix inequality problem. We apply the standard and spherical μ tools to a flight control problem. Through the numerical study, it is shown that spherical μ is less conservative than standard μ. The main contributions are the following: 1) An upper bound is developed for spherical μ. 2) It is shown that the use of spherical μ is rationalized from a statistical perspective. 3) The newly derived upper bound is applied to the robust stability analysis of a flight control system.

I. Introduction

STABILIZING a closed-loop system is the most elementary objective of feedback control. Nevertheless, in practice, stability is sometimes lost while feedback control systems work. The factors threatening the stability of a feedback system are the differences between a physical plant in operation and a mathematical model for controller design. Some differences are caused by high-order dynamics or nonlinearities that are neglected for simplification, and others can be regarded as variations of parameters included in a design model. One of the most basic problems in robust control is to determine whether a feedback system remains stable against those various uncertainties. If a feedback system is stable for all elements in a given uncertainty set, it is said that the system achieves robust stability.

The structured singular value [(SSV) or μ] and the multivariable stability margin (or k_m) were simultaneously developed as robustness measures for linear systems subject to structured, linear time-invariant (LTI) perturbations.[1,2] In short, k_m means the size of the smallest uncertainty that makes a closed-loop system unstable, and μ is defined as the reciprocal of k_m. According to these original definitions, the uncertainty size is measured by the largest singular value of a block-diagonal matrix that describes uncertainty. If a perturbation matrix is normalized such that the largest singular value is less than one, the problem of proving robust stability becomes equivalent to determining whether μ is one or less for all frequencies. This is referred to as the small-μ theorem.[3,4]

In this paper, we direct our attention only to real parametric uncertainties. When uncertainty consists of only real parameters, the SSV is, in particular, called real μ. In this case, the largest singular value of a perturbation matrix is equal to the maximum (or ℓ_∞) norm of the vector comprising uncertain parameters. An inequality constraint with respect to the maximum norm, which is equivalent to interval constraints on individual uncertain elements, defines a hypercube in a multidimensional space of uncertain parameters. Therefore, stability must be preserved everywhere inside of a cubical domain so that a system can pass the robust stability test based on the standard μ tools.[5] In general, the vertices of a perturbation cube are termed worst-on-worst combinations of uncertainties. In the real engineering world, however, there certainly exist cases where the conventional worst-on-worst approach is too conservative. This difficulty is due to the use of the maximum norm to measure parameter variations.

From the motive just mentioned, we consider parametric uncertainties that are restricted to a hypersphere in a parameter space. This constraint is represented by an inequality with respect to the Euclidean (or ℓ_2) norm of a parameter vector. Because a hypersphere with the unit Euclidean norm is inscribed to a hypercube with the unit maximum norm, it should become easy to satisfy the requirement of robust stability. For such a spherical uncertainty set, we define an extended version of real μ. This extension of μ is referred to as "spherical (real) μ" throughout the paper. The reciprocal of spherical μ means the radius of a guaranteed stable spherical domain. Khatri and Parrilo[6] and Parrilo and Khatri[7] recently studied a spherical complex μ problem where a perturbation matrix consists of nonrepeated, complex uncertain parameters. We extend their work to a more practical problem subject to possibly repeated, real uncertain parameters. We newly develop an upper bound of spherical real μ. This is similar to a well-known upper bound of standard μ developed by Fan et al.[8] In robustness analysis, upper bounds of μ are usually used because they provide sufficient conditions for robust stability. It should be noted that El Ghaoui et al.[9] and El Ghaoni[10] addressed a lower bound of spherical μ for parametric uncertainties, though the term of spherical μ was not used.

For a numerical comparison between spherical and standard μ, both of them are applied to an engineering problem. We examine the robust stability of an automatic landing control system for an uninhabited reentry vehicle. The verification of flight control systems against uncertainty would be one of the problems in which μ analysis plays an important role. Other applications of μ to flight control problems are found in several references.[11–16]

The main contributions of the paper are the following: 1) An upper bound is developed for spherical μ. 2) It is shown that the use of spherical μ is rationalized from a statistical perspective. 3) The newly derived upper bound is applied to the robust stability analysis of a flight control system.

This paper is organized as follows. Section II describes the framework of real μ analysis and presents an engineering reason justifying the use of the Euclidean norm instead of the conventional maximum norm. Section III reviews standard μ for completeness. In Sec. IV, we define spherical μ and develop its upper bound. Section V provides an example problem. In Sec. VI, we make a comparison between standard and spherical μ based on the numerical results. Section VII presents some concluding remarks. Finally,

Received 20 December 2001; revision received 7 May 2002; accepted for publication 19 June 2002.

*Senior Researcher, Flight Systems Research Center, Chofu. Member AIAA.
†Senior Researcher, Space Technology Research Center, Chofu.

the Appendix gives state-space data so that the interested reader can reproduce analysis results.

II. Preliminaries

A. Notation

We denote the sets of positive integers, real numbers, and complex numbers by $\boldsymbol{N}$, $\boldsymbol{R}$, and $\boldsymbol{C}$, respectively. We denote the $n \times n$ identity matrix by I_n. If M is a matrix, M^T and M^H stand for the transpose and the complex conjugate transpose of M, respectively. This applies to a vector as well. When c is a complex number, $\bar{c}$ stands for the complex conjugate of c. For any matrix M, $\bar{\sigma}(M)$ denotes the largest singular value of M and $\det(M)$ the determinant of M. For a real symmetric matrix $M = M^T \in \boldsymbol{R}^{n \times n}$, $M > 0$ and $M \geq 0$ denote $x^T M x > 0$ and $x^T M x \geq 0$ for all nonzero $x \in \boldsymbol{R}^n$, respectively. Similarly, for a Hermitian matrix $M = M^H \in \boldsymbol{C}^{n \times n}$, $M > 0$ and $M \geq 0$ denote $x^H M x > 0$ and $x^H M x \geq 0$ for all nonzero $x \in \boldsymbol{C}^n$, respectively. For a real vector $x \in \boldsymbol{R}^n$, $\|x\|_2$ denotes the Euclidean (or ℓ_2) norm of x, that is, $\|x\|_2 = \sqrt{(x^T x)}$, and $\|x\|_\infty$ denotes the maximum (or ℓ_∞) norm of x, that is, $\|x\|_\infty = \max_i(|x_i|)$. A block-diagonal matrix with $A_1, A_2, \ldots, A_n$ on the diagonal is denoted by $\mathrm{diag}(A_1, A_2, \ldots, A_n)$. Finally, j denotes $\sqrt{-1}$.

B. Framework of Real μ Analysis

Figure 1 shows the standard block diagram for μ analysis. In general, the matrix $M \in \boldsymbol{C}^{n \times n}$ is the frequency response of a transfer matrix that describes a nominal closed-loop system. We can assume M to be stable without loss in generality. The matrix $\Delta \in \boldsymbol{R}^{n \times n}$ represents uncertainty included in the system. In this paper, we consider only constant, real, parametric uncertainties, and we assume that Δ belongs to the set

$$\boldsymbol{\Delta} = \left\{ \mathrm{diag}\left(\delta_1 I_{r_1}, \delta_2 I_{r_2}, \ldots, \delta_m I_{r_m}\right) \middle| \delta_i \in \boldsymbol{R} \right\} \tag{1}$$

where $r_1, r_2, \ldots, r_m$ are positive integers such that

$$r_1 + r_2 + \cdots + r_m = n \tag{2}$$

In the succeeding discussions, we employ the parameter vector

$$\delta = [\delta_1, \delta_2, \ldots, \delta_m]^T \in \boldsymbol{R}^m \tag{3}$$

along with the matrix Δ as a description of uncertainty. In addition, we define the vector r as

$$r = [r_1, r_2, \ldots, r_m]^T \in \boldsymbol{N}^m \tag{4}$$

for describing the block structure of Δ.

C. Uncertainty Model

In this paper, unlike the literature on real μ, we regard δ as a zero-mean Gaussian-distributed random vector with the covariance

$$S = s^{-2} I_m \tag{5}$$

where s is a positive real number. As is known from S being a diagonal matrix, any elements of δ are assumed to be statistically independent. Additionally, each element of δ is normalized such that the s–σ value (the standard deviation multiplied by s) is equal to one. Note that any m-dimensional correlated Gaussian random vector with a nonzero mean value can be defined as an affine function of δ. Therefore, the assumption on the covariance in Eq. (5) has generality.

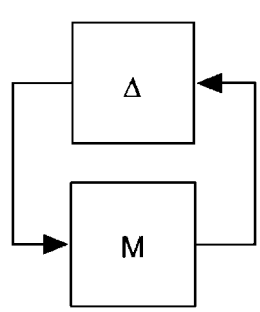

Fig. 1 Standard interconnection structure for μ analysis.

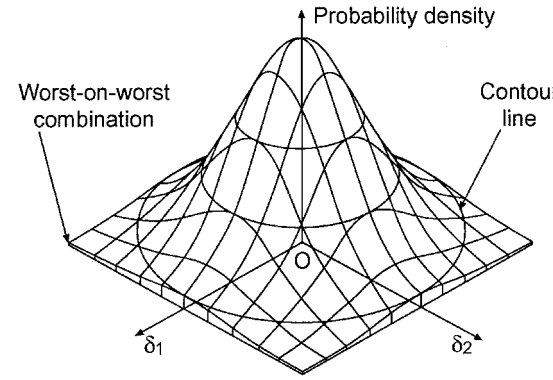

Fig. 2 Probability density in two-dimensional case.

D. Interval and Spherical Constraints

Let us consider constraints on δ that define uncertainty domains where the system in Fig. 1 should remain stable. A conventional approach is to handle interval constraints on individual scalar components:

$$|\delta_i| < 1, \qquad i = 1, 2, \ldots, m \iff \|\delta\|_\infty < 1 \tag{6}$$

Componentwise interval constraints are equivalent to an inequality constraint with respect to the maximum norm. Interval constraints would be appropriate if δ consisted of uniform-distributed random variables or deterministic variables that define an operating envelope. The inequalities in Eq. (6) define a hypercube in the δ space, which includes worst-on-worst combinations of uncertainties. However, because we assume δ to be a Gaussian random vector and a value of more than three is usually assigned to s in most engineering problems, such worst-on-worst combinations rarely occur. This is illustrated by the probability density of δ in Fig. 2. Thus we need a more realistic constraint on δ.

As understood from Fig. 2, the most meaningful constraint on δ would be one with respect to the probability density of δ. Such a constraint excludes combinations of rare occurrence. Specifically, the region where the probability density of δ is greater than the s–σ level becomes a hypersphere with the unit radius, which is written as

$$\delta^T S^{-1} \delta < s^2 \iff \|\delta\|_2 < 1 \tag{7}$$

These inequalities reveal that a spherical constraint on δ has a clear statistical meaning, and this justifies the use of the Euclidean norm to measure the size of δ. We consider the system in Fig. 1 to be robustly stable if it is stable for all δ such that $\|\delta\|_2 < 1$.

III. Standard μ

In this section, we review standard real μ for comparison with spherical μ, which is defined later.

A. Definition of Standard μ

Definition 1: The standard structured singular value $\mu_\infty(M)$ of a complex matrix $M \in \boldsymbol{C}^{n \times n}$ with respect to a block structure $r \in \boldsymbol{N}^m$ is defined to be 0 if $I_n - \Delta M$ is nonsingular for all $\Delta \in \boldsymbol{\Delta}$ and

$$\mu_\infty(M) = 1/\min\{\|\delta\|_\infty | \Delta \in \boldsymbol{\Delta}, \det(I_n - \Delta M) = 0\} \tag{8}$$

otherwise. □

As seen from Eq. (8), $1/\mu_\infty$ means the size of the minimum hypercube that makes $I_n - \Delta M$ singular. Because $\|\delta\|_\infty = \max_i(|\delta_i|) = \bar{\sigma}(\Delta)$, nonzero μ_∞ can be written as

$$\mu_\infty(M) = 1/\min\{\bar{\sigma}(\Delta) | \Delta \in \boldsymbol{\Delta}, \det(I_n - \Delta M) = 0\} \tag{9}$$

where $\bar{\sigma}(\,)$ stands for the largest singular value. This expression is identical with the original definition of μ by Doyle.[1]

B. Upper Bound of Standard μ

As the small-μ theorem[3,4] claims, the closed-loop system in Fig. 1 is stable for all $\Delta \in \boldsymbol{\Delta}$ subject to $\|\delta\|_\infty < 1$ if and only if

$$\sup_{\omega \in R} \mu_\infty[M(j\omega)] \leq 1 \tag{10}$$

Unfortunately, it is probable that there are not polynomial-time algorithms to compute an exact value of μ_∞. This means that computing μ_∞ itself is intractable unless the problem sizes n and m are very limited. To avoid this difficulty, we usually use upper bounds of μ_∞ that can be computed in polynomial time, because μ upper bounds provide sufficient conditions for the robust stability criterion in Eq. (10). A well-known upper bound of μ_∞ is the one that was developed by Fan et al.[8] Denoted by $\bar{\mu}_\infty$, the upper bound is defined as

$$\bar{\mu}_\infty(M) = \inf_{D \in \boldsymbol{D}, G \in \boldsymbol{G}} \{\alpha > 0 | M^H D M + j(GM - M^H G) - \alpha^2 D < 0\} \tag{11}$$

where

$$\boldsymbol{D} = \left\{ \mathrm{diag}(D_1, D_2, \ldots, D_m) > 0 \middle| D_i = D_i^H \in \boldsymbol{C}^{r_i \times r_i} \right\} \tag{12}$$

$$\boldsymbol{G} = \left\{ \mathrm{diag}(G_1, G_2, \ldots, G_m) \middle| G_i = G_i^H \in \boldsymbol{C}^{r_i \times r_i} \right\} \tag{13}$$

Computing $\bar{\mu}_\infty$ is formulated into the following generalized eigenvalue minimization problem (GEVP) subject to linear matrix inequality (LMI) constraints[17]:

Minimize α^2 subject to

$$0 < D, \qquad M^H D M + j(GM - M^H G) < \alpha^2 D \tag{14}$$

This optimization problem can be solved using efficient polynomial-time algorithms based on interior point methods.[18,19]

For verifying robust stability exactly, the optimization problem in Eq. (14) must be solved for all frequencies. In practice, such things are impossible to execute. A common practice is to compute $\bar{\mu}_\infty[M(j\omega)]$ at a finite number of frequency grids. However, it is known that real μ upper bounds can be discontinuous functions of frequency. Consequently, it is possible to miss sharp peaks between frequency grids. Feron proposed a heuristic technique to bypass this issue.[20] Feron's method slightly modifies the optimization problem in Eq. (14) so that the second constraint can be satisfied at the neighboring two frequencies.

IV. Spherical μ

In this section, we formally define spherical μ and develop its upper bound for numerical analysis.

A. Definition of Spherical μ

Definition 2: The spherical structured singular value $\mu_2(M)$ of a complex matrix $M \in \boldsymbol{C}^{n \times n}$ with respect to a block structure $r \in \boldsymbol{N}^m$ is defined to be 0 if $I_n - \Delta M$ is nonsingular for all $\Delta \in \boldsymbol{\Delta}$ and

$$\mu_2(M) = 1/\min\{\|\delta\|_2 | \Delta \in \boldsymbol{\Delta}, \det(I_n - \Delta M) = 0\} \tag{15}$$

otherwise. □

Geometrically, $1/\mu_2$ denotes the radius of the minimum hypersphere that makes $I_n - \Delta M$ singular, that is, the size of a guaranteed stable region measured by the Euclidean norm. Figure 3 compares μ_2 with μ_∞ in a two-dimensional case.

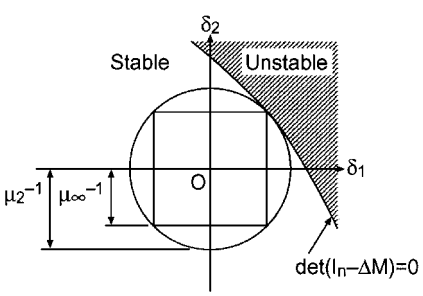

Fig. 3 Geometrical comparison of standard and spherical μ.

B. Upper Bound of Spherical μ

Like μ_∞, it would be difficult to compute an exact value of μ_2. Alternatively, we provide a tractable upper bound of μ_2 in the form similar to Eq. (11). The main result of this paper is summarized into the following theorem.

Theorem (main result): For a matrix $M \in \boldsymbol{C}^{n \times n}$ and a block structure $r \in \boldsymbol{N}^m$, define $\bar{\mu}_2(M)$ as

$$\bar{\mu}_2(M) = \inf_{F \in \boldsymbol{F}, G \in \boldsymbol{G}} \left\{ \alpha > 0 \middle| M^H \left(F \overset{r}{\circ} I_m\right) M + j(GM - M^H G) - \alpha^2 F < 0 \right\} \tag{16}$$

where

$$\boldsymbol{F} = \{F | F \in \boldsymbol{C}^{n \times n}, \qquad F = F^H > 0\} \tag{17}$$

Then, the following inequality holds:

$$\mu_2(M) \leq \bar{\mu}_2(M) \tag{18}$$

□

We can obtain a numerical value of $\bar{\mu}_2$ by solving an equivalent LMI problem with respect to α^2, F, and G. A MATLAB® program can be easily implemented using commands from the LMI Control Toolbox.[19]

In the theorem, a special operator depending on a block structure is employed. For two matrices $A \in \boldsymbol{C}^{n \times n}$ and $B \in \boldsymbol{C}^{m \times m}$ that relate through a block-structure $r \in \boldsymbol{N}^m$ such that

$$\sum_{i=1}^{m} r_i = n$$

the product $A \overset{r}{\circ} B$ is defined as

$$A \overset{r}{\circ} B = \begin{bmatrix} A_{11}b_{11} & A_{12}b_{12} & \cdots & A_{1m}b_{1m} \\ A_{21}b_{21} & A_{22}b_{22} & \cdots & A_{2m}b_{2m} \\ \vdots & \vdots & \ddots & \vdots \\ A_{m1}b_{m1} & A_{m2}b_{m2} & \cdots & A_{mm}b_{mm} \end{bmatrix} \tag{19}$$

where $A_{ik} \in \boldsymbol{C}^{r_i \times r_k}$ is the (i,k) block of A and $b_{ik} \in \boldsymbol{C}$ is the (i,k) element of B. This product is an extension of the Hadamard elementwise product of two matrices (see Ref. 6).

To prove the theorem, we employ the following three lemmas.

Lemma 1 (Schur complement) (see Ref. 18): Let $P = P^T$, $Q = Q^T$, and R be real matrices. The LMI

$$\begin{bmatrix} P & R \\ R^T & Q \end{bmatrix} > 0 \tag{20}$$

is equivalent to

$$Q > 0, \qquad P - RQ^{-1}R^T > 0 \tag{21}$$

□

Lemma 2: Let $A \in \boldsymbol{C}^{n \times n}$ and $B \in \boldsymbol{C}^{m \times m}$. If $A > 0$ and $B \geq 0$, then $A \overset{r}{\circ} B \geq 0$. □

Proof of Lemma 2: If $B \geq 0$, there exists a matrix C such that $CC = B$, $C = C^H$, and $C \geq 0$. Therefore, the (i,k) element of B is written as

$$\begin{aligned} b_{ik} &= c_{i1}c_{1k} + c_{i2}c_{2k} + \cdots + c_{im}c_{mk} \\ &= c_{i1}\bar{c}_{k1} + c_{i2}\bar{c}_{k2} + \cdots + c_{im}\bar{c}_{km} \\ &= \sum_{l=1}^{m} c_{il}\bar{c}_{kl} \end{aligned} \tag{22}$$

where c_{il} is the (i, l) element of C and $\bar{c}_{kl}$ is the complex conjugate of c_{kl}. As a result, we have

$$A \overset{r}{\circ} B = \sum_{l=1}^{m} A \overset{r}{\circ} \left(\begin{bmatrix} c_{1l} \\ c_{2l} \\ \vdots \\ c_{ml} \end{bmatrix} \begin{bmatrix} c_{1l} \\ c_{2l} \\ \vdots \\ c_{ml} \end{bmatrix}^H \right)$$

$$= \sum_{l=1}^{m} \operatorname{diag}\left(c_{1l} I_{r_1}, c_{2l} I_{r_2}, \ldots, c_{ml} I_{r_m}\right) A \operatorname{diag}\left(c_{1l} I_{r_1}, c_{2l} I_{r_2}, \ldots, c_{ml} I_{r_m}\right)^H \tag{23}$$

Note that, for any matrix $X \in \boldsymbol{C}^{n \times n}$, $XAX^H \geq 0$ holds if $A > 0$. Consequently, it has been shown that $A \overset{r}{\circ} B \geq 0$ if $A > 0$ and $B \geq 0$. □

Lemma 3 (multiplier)[21,22]: A matrix $T \in \boldsymbol{C}^{n \times n}$ is nonsingular if there exists a matrix $C \in \boldsymbol{C}^{n \times n}$ such that $CT + T^H C^H > 0$. □

Here we provide the proof of the theorem. This is based on the same idea as that used for proving $\bar{\mu}_\infty$ by Meinsma et al.[22]

Proof of theorem: Let $C = \alpha^2 F + jM^H G$ for some $F \in \boldsymbol{F}$, $G \in \boldsymbol{G}$, and $\alpha > 0$. Then, we have

$$\begin{aligned} C(I_n - \Delta M) + (I_n - \Delta M)^H C^H &= -\Psi_\alpha(F, G) + M^H \left(F \overset{r}{\circ} I_m\right) M + \alpha^2 F \\ &\quad - \alpha^2 (F \Delta M + M^H \Delta F) \\ &= -\Psi_\alpha(F, G) + M^H \left(F \overset{r}{\circ} I_m\right) M - \alpha^2 M^H \Delta F \Delta M \\ &\quad + \alpha^2 (I_n - \Delta M)^H F (I_n - \Delta M) \\ &= -\Psi_\alpha(F, G) + M^H \left[F \overset{r}{\circ} \left(I_m - \alpha^2 \delta \delta^T\right)\right] M \\ &\quad + \alpha^2 (I_n - \Delta M)^H F (I_n - \Delta M) \end{aligned} \tag{24}$$

where

$$\Psi_\alpha(F, G) = M^H \left(F \overset{r}{\circ} I_m\right) M + j(GM - M^H G) - \alpha^2 F \tag{25}$$

For deriving Eq. (24), we used that $\Delta = \Delta^H$ and $G\Delta = \Delta G$ for every $\Delta \in \boldsymbol{\Delta}$.

Applying Lemma 1, we obtain

$$\begin{aligned} \|\delta\|_2 \leq \frac{1}{\alpha} &\iff \frac{1}{\alpha^2} - \delta^T I_m^{-1} \delta \geq 0 \\ &\iff \begin{bmatrix} I_m & \delta \\ \delta^T & \dfrac{1}{\alpha^2} \end{bmatrix} \geq 0 \\ &\iff I_m - \alpha^2 \delta \delta^T \geq 0 \end{aligned} \tag{26}$$

Because $F > 0$, it follows from Lemma 2 that $F \overset{r}{\circ} (I_m - \alpha^2 \delta \delta^T) \geq 0$ for all $\Delta \in \boldsymbol{\Delta}$ such that $\|\delta\|_2 \leq 1/\alpha$. Consequently, it can be claimed that

$$M^H \left[F \overset{r}{\circ} \left(I_m - \alpha^2 \delta \delta^T\right)\right] M \geq 0 \tag{27}$$

if $\|\delta\|_2 \leq 1/\alpha$.

As a result, from Eq. (24), we have

$$C(I_n - \Delta M) + (I_n - \Delta M)^H C^H > 0 \quad \text{for all} \quad \Delta \in \boldsymbol{\Delta} \text{ subject to } \|\delta\|_2 \leq 1/\alpha \tag{28}$$

if $\Psi_\alpha(F, G) < 0$. It follows from Lemma 3 that

$$(I_n - \Delta M) \text{ is nonsingular for all } \Delta \in \boldsymbol{\Delta} \text{ subject to } \|\delta\|_2 \leq 1/\alpha \tag{29}$$

if Eq. (28) holds. By the definition of μ_2 in Eq. (15), it is verified that $\mu_2(M) < \alpha$ if Eq. (29) holds. Eventually, we have proved that $\mu_2(M) < \alpha$ if $\Psi_\alpha(F, G) < 0$.

Because $\bar{\mu}_2(M)$ is the infimum of α over all $F \in \boldsymbol{F}$ and $G \in \boldsymbol{G}$ that satisfy $\Psi_\alpha(F, G) < 0$, the inequality in Eq. (18) obviously holds. □

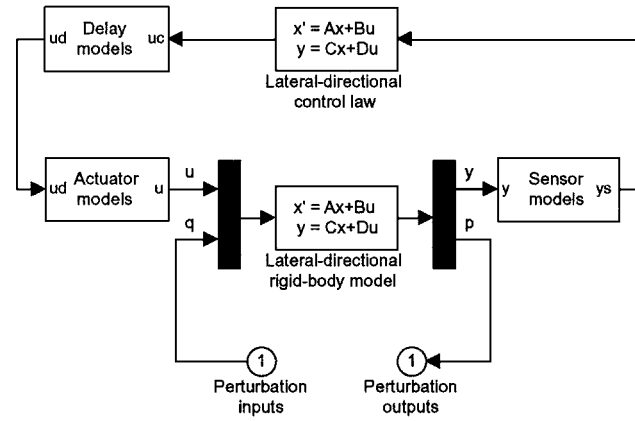

Fig. 4 Block diagram of example flight control system.

V. Example Problem: Automatic Landing Control System

In this section and the next, we apply the standard and spherical μ tools to a practical flight control problem. We deal with an automatic landing control system for an uninhabited reentry vehicle. In general, the aircraft linearized equations of motion can be separated into the longitudinal and lateral–directional systems, and here we take up a lateral–directional control system, which includes more uncertain parameters. Figure 4 shows the Simulink block diagram for robust stability analysis. The perturbation matrix Δ is inserted between the input and output ports. This block diagram can be easily transformed into the plant matrix M for μ analysis in Fig. 1. Each block will be explained in detail later. Although actual sensors installed on a vehicle measure not only rigid-body motion, but also structural vibration, the analysis model in Fig. 4 ignores a structural model for simplification. Therefore, the stability analysis based on this model is valid only for a low-frequency range up to about 10 Hz, where structural dynamics do not have serious effects.

A. Lateral–Directional Rigid-Body Model with Uncertainty

The states x, measured outputs y, and control inputs u of the lateral–directional rigid-body model in Fig. 4 are as follows:

$$x = \begin{bmatrix} v \\ p \\ \phi \\ r \end{bmatrix} = \begin{bmatrix} \text{lateral velocity (m/s)} \\ \text{roll rate (rad/s)} \\ \text{bank angle (rad)} \\ \text{yaw rate (rad/s)} \end{bmatrix} \tag{30}$$

$$y = \begin{bmatrix} \phi \\ a_y \\ p \\ r \end{bmatrix} = \begin{bmatrix} \text{bank angle (rad)} \\ \text{lateral acceleration (m/s}^2\text{)} \\ \text{roll rate (rad/s)} \\ \text{yaw rate (rad/s)} \end{bmatrix} \tag{31}$$

$$u = \begin{bmatrix} \delta_a \\ \delta_r \end{bmatrix} = \begin{bmatrix} \text{aileron deflection (rad)} \\ \text{rudder deflection (rad)} \end{bmatrix} \tag{32}$$

We consider uncertainty in nine nondimensional aerodynamic derivatives. The lateral–directional model including the uncertain derivatives can be described in the form of the state-space linear fractional representation (LFR):

$$\begin{bmatrix} \dot{x} \\ y \end{bmatrix} = \left(\begin{bmatrix} A & B_1 \\ C_1 & D_{11} \end{bmatrix} + \begin{bmatrix} B_2 \\ D_{12} \end{bmatrix} \Delta (I_{11} - D_{22} \Delta)^{-1} \begin{bmatrix} C_2 & D_{21} \end{bmatrix} \right) \times \begin{bmatrix} x \\ u \end{bmatrix} \tag{33}$$

where

$$\Delta = \operatorname{diag}(\delta_1, \delta_2, \ldots, \delta_7, \delta_8 I_2, \delta_9 I_2) \tag{34}$$

In this case, we have $D_{22}=0$, and the right-hand side of Eq. (33) depends affinely on Δ. The LFR in Eq. (33) is equivalent to the linear system with the fictitious output feedback:

$$\begin{bmatrix} \dot{x} \\ y \\ q \end{bmatrix} = \begin{bmatrix} A & B_1 & B_2 \\ C_1 & D_{11} & D_{12} \\ C_2 & D_{21} & D_{22} \end{bmatrix} \begin{bmatrix} x \\ u \\ p \end{bmatrix}, \qquad p = \Delta q \tag{35}$$

where p and q are the perturbation inputs and outputs, respectively. Note that this representation is used in Fig. 4.

The parametric uncertainties $\delta_1, \delta_2, \ldots, \delta_9$ are assumed to be Gaussian random variables such that each 3-σ value is equal to one. In other words, s in Eq. (5) is assumed to be 3. We let $\delta_1, \delta_2, \ldots, \delta_7$ correspond to the variations of the nondimensional aerodynamic derivatives C_{y_β}, C_{l_β}, C_{n_β}, $C_{y_{\delta_a}}$, $C_{l_{\delta_a}}$, $C_{n_{\delta_a}}$, and $C_{y_{\delta_r}}$, respectively. The remaining uncertain parameters are used to define the correlated variations of $C_{l_{\delta_r}}$ and $C_{n_{\delta_r}}$, which have a correlation coefficient of -0.9 and are written as

$$\begin{bmatrix} \Delta C_{l_{\delta_r}} \big/ \left(3\sigma_{C_{l_{\delta_r}}}\right) \\ \Delta C_{n_{\delta_r}} \big/ \left(3\sigma_{C_{n_{\delta_r}}}\right) \end{bmatrix} = \begin{bmatrix} 0.8473 & -0.5311 \\ -0.5311 & 0.8473 \end{bmatrix} \begin{bmatrix} \delta_8 \\ \delta_9 \end{bmatrix} \tag{36}$$

where $\Delta C_{l_{\delta_r}}$ and $\Delta C_{n_{\delta_r}}$ are the variations and $\sigma_{C_{l_{\delta_r}}}$ and $\sigma_{C_{n_{\delta_r}}}$ are the standard deviations of $C_{l_{\delta_r}}$ and $C_{n_{\delta_r}}$, respectively. For the definitions of the aerodynamic derivatives, refer to textbooks on flight dynamics, for example, Ref. 23.

B. Sensor, Actuator, and Time Delay Models

Sensors and actuators are modeled as the following first-order systems with the identical time constants:

$$\text{sensor}: [1/(0.04s+1)]I_4, \qquad \text{actuator}: [1/(0.04s+1)]I_2 \tag{37}$$

For transport delay, we employ the first-order Padé approximation with a delay time of 50 ms:

$$\text{time delay}: \frac{1-0.025s}{1+0.025s} I_2 \tag{38}$$

C. Lateral–Directional Control Law

The controller examined in this example is a gain-scheduled one with guaranteed $\mathcal{H}_\infty$ performance.[24] For controller design, the equation of lateral–directional motion was regarded as a linear parameter varying (LPV) polytopic plant, which is a convex combination of separate state-space plants at "vertex points" that overbound an operating range. Table 1 summarizes the flight conditions at vertex points used for controller design. The control law is also given as an LPV polytopic system, that is, a convex interpolation of vertex controllers. Linear interpolation is made with respect to a measurable scheduling parameter. In our case, Mach number was selected for gain scheduling. By solving an LMI problem, we obtained the vertex controllers minimizing closed-loop $\mathcal{H}_\infty$ performance. See Refs. 19 and 25 for details. Although the performance objective included high-frequency gain attenuation, any structured uncertainties were not considered. For this reason, we decided to analyze the stability robustness of the closed-loop system in this study. Robust stability analysis was performed for LTI systems at the same vertex points as those used in design with the scheduling parameter frozen.

Table 1 Flight conditions at vertex points

Case number	Altitude, m	Mach number	Angle of attack, deg
1	3000	0.493	3.02
2	800	0.400	3.48
3	200	0.365	6.29
4	10	0.244	9.26

VI. Analysis Results

Figure 5 shows the results of robust stability μ analysis. In each plot in Fig. 5, the standard μ upper bound is depicted along with the spherical μ upper bound. The purpose of this comparison is to evaluate how conservative the newly derived spherical μ upper bound is. Because the Feron method[20] did not detect any discontinuities with respect to frequency, we present the μ upper bounds obtained from the original GEVPs. We also computed standard μ lower bounds using the MATLAB μ-Analysis and Synthesis Toolbox.[5] In every case, the gap between the peak values of the standard μ upper and lower bounds is small. From these results, it turns out that the spherical μ upper bound is much less conservative than the standard μ upper and lower bounds. Standard μ means the size of a guaranteed stable hypercube in a parameter space. As can be understood from Fig. 3, when such a hypercube touches an unstable region at a point far from any of the axes, standard μ becomes conservative in comparison with spherical μ. This explains the reason why the standard μ results are very conservative in this example.

It is said that, in general, μ analysis is conservative compared with Monte Carlo analysis. To assess the conservativeness of the spherical μ upper bound from a probabilistic viewpoint, we conducted Monte Carlo analysis.[26,27] For each case, we computed the probability of stability based on 50,000 random data points generated from the Gaussian probability density function. Table 2 compares the peak values of standard and spherical μ upper bounds with the probability of stability. In cases 3 and 4, the peak values of spherical μ are almost equal to one, and the probability of stability estimates are more than 99.9%. These probabilities seem satisfactory for this example because the reentry vehicle considered here is uninhabited. However, they may be insufficient for inhabited vehicles. This comparison suggests that the newly derived spherical μ upper bound is not conservative even in comparison with the probability measure

Table 2 Numerical comparison of μ peak values and probability of stability

Case number	μ analysis		Probability of stability, %
	$\max_\omega(\bar{\mu}_\infty)$	$\max_\omega(\bar{\mu}_2)$	
1	2.4290	1.1343	99.724
2	3.4541	1.5545	97.582
3	2.0374	0.9894	99.940
4	2.0956	0.9852	99.942

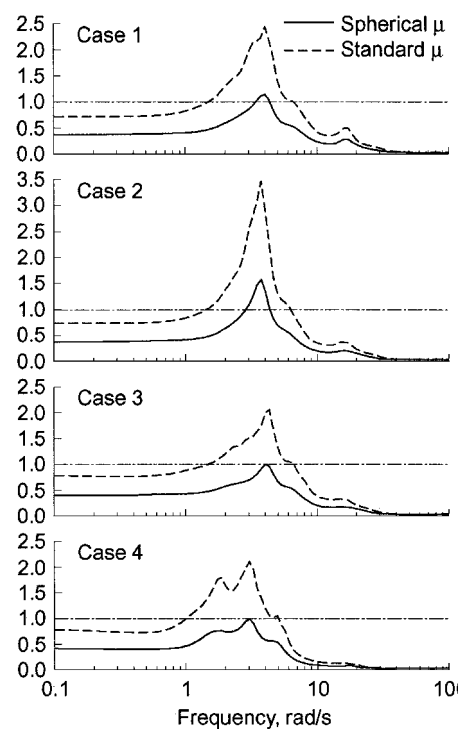

Fig. 5 Results of robust stability μ analysis.

and can be used as a realistic robustness measure by choosing an appropriate value for s in Eq. (5).

VII. Conclusions

In this paper, we have described spherical μ for the robust stability analysis of linear control systems subject to real parametric uncertainties. Spherical μ is an extended version of the real structured singular value. Geometrically, the reciprocal of spherical μ means the size of a guaranteed stable hypersphere. We have noted that the use of spherical μ is rationalized if uncertain parameters are Gaussian-distributed random variables. The primary contribution of this paper is the development of an upper bound of spherical μ, which can be computed using efficient LMI software. Through a practical numerical example, it has been shown that the spherical μ upper bound is less conservative than the standard μ upper and lower bounds. Furthermore, we have found that the newly derived spherical μ upper bound is not conservative even in comparison with the probability measure given by Monte Carlo analysis. Because uncertainties are often assumed to be Gaussian variables in real engineering problems, the spherical μ upper bound can be widely used in place of the standard μ upper and lower bounds.

Appendix: State-Space Data

The lateral–directional rigid-body model is

$$P = \left[\begin{array}{c|cc} A & B_1 & B_2 \\ \hline C_1 & D_{11} & D_{12} \\ C_2 & D_{21} & D_{22} \end{array}\right]$$

where $A \in \boldsymbol{R}^{4\times 4}$, $B_1 \in \boldsymbol{R}^{4\times 2}$, $B_2 \in \boldsymbol{R}^{4\times 11}$, $C_1 \in \boldsymbol{R}^{4\times 4}$, $C_2 \in \boldsymbol{R}^{11\times 4}$, $D_{11} \in \boldsymbol{R}^{4\times 2}$, $D_{12} \in \boldsymbol{R}^{4\times 11}$, $D_{21} \in \boldsymbol{R}^{11\times 2}$, and $D_{22} \in \boldsymbol{R}^{11\times 11}$. This model contains the state-space matrices A, B_1, C_1, and D_{11} to represent the nominal relation between the control inputs and measured outputs and has the five fictitious matrices, B_2, C_2, D_{12}, D_{21}, and D_{22}, to describe uncertainty in the aerodynamic coefficients; refer to Eq. (35). The lateral–directional control law frozen at a flight condition is described by the state-space model

$$K = \left[\begin{array}{c|c} A_K & B_K \\ \hline C_K & D_K \end{array}\right]$$

where $A_K \in \boldsymbol{R}^{16\times 16}$, $B_K \in \boldsymbol{R}^{16\times 4}$, $C_K \in \boldsymbol{R}^{2\times 16}$, and $D_K \in \boldsymbol{R}^{2\times 4}$. The state-space data of P and K for case 1 (see Table 1) are given in

```
P =
  Columns 1 through 6
      -0.329         8.44          8.5       -161.7        -6.14        14.72
     -0.1734       -1.621            0       0.1342        -40.2        11.41
           0            1            0       -0.577            0            0
    -0.00871       0.0596            0       -0.407       0.0793        -2.66
           0            0            1            0            0            0
      -0.329    -0.094896     0.007192     0.075015        -6.14        14.72
           0            1            0            0            0            0
           0            0            0            1            0            0
           1            0            0            0            0            0
           1            0            0            0            0            0
           1            0            0            0            0            0
           0            0            0            0            1            0
           0            0            0            0            1            0
           0            0            0            0            1            0
           0            0            0            0            0            1
           0            0            0            0            0            1
           0            0            0            0            0            1
           0            0            0            0            0            1
  Columns 7 through 12
    0.080236            0            0       11.191            0            0
           0     0.045176    0.0012516            0       5.6227      0.22012
           0            0            0            0            0            0
           0    0.0017686    0.0049248            0      0.22012      0.86613
           0            0            0            0            0            0
    0.080236            0            0       11.191            0            0
           0            0            0            0            0            0
           0            0            0            0            0            0
           0            0            0            0            0            0
           0            0            0            0            0            0
           0            0            0            0            0            0
           0            0            0            0            0            0
           0            0            0            0            0            0
           0            0            0            0            0            0
           0            0            0            0            0            0
           0            0            0            0            0            0
           0            0            0            0            0            0
           0            0            0            0            0            0
           0            0            0            0            0            0
  Columns 13 through 17
      4.4766            0            0            0            0
           0       1.8104   -0.086509      -1.1347      0.13802
           0            0            0            0            0
           0     0.070875     -0.34039   -0.044423      0.54308
           0            0            0            0            0
      4.4766            0            0            0            0
           0            0            0            0            0
           0            0            0            0            0
           0            0            0            0            0
           0            0            0            0            0
           0            0            0            0            0
           0            0            0            0            0
           0            0            0            0            0
           0            0            0            0            0
           0            0            0            0            0
           0            0            0            0            0
           0            0            0            0            0
           0            0            0            0            0
           0            0            0            0            0
```

Fig. A1 Lateral–directional rigid-body model for case 1.

```
K =
  Columns 1 through 6
      -6.3048      -2.7538       6.1397      -3.0387       5.6256       0.7841
       -114.3       61.123       99.807      -38.116      -12.708      -2.0389
      -633.33       5.1817        102.1       27.685       8.1866     -0.77701
      -6.5215      -104.15       18.844       -18.84       -3.802      0.58493
      -291.75       151.62      -2.5425      -5.3594      -2.8386      0.92513
      -3.4421       5.3497    -0.22962      -1.0164      0.66214       -10.298
       1.2972       56.243       0.9014      -12.597      -1.5334      -6.3142
       956.45      -1299.5      -10.541      -1.7938      -18.526     -0.72806
       703.71       189.96       -15.27       11.151   -0.069065      -9.0921
       1800.7       283.66      -33.895       5.4786      -9.8901       4.1134
      -953.13       1057.4       10.362       1.0974       1.9007      -2.0535
      -518.41       1800.2      -46.693       21.463       3.2538      0.26487
       3118.1       238.05       32.243        4.975        7.089      0.40415
      -727.17       7.6358       87.739       18.446       4.8513     -0.56343
      -216.57       417.58        90.37       -67.62       -18.56       2.1132
      -1958.6       233.08      -73.174       161.51       4.4311      -2.4643
      -1.0933      -3.9437    0.033923    0.0056871   -0.019971   -0.00028302
       6.6651      -1.4538   -0.095495     0.012875   -0.043874   -0.00011129
  Columns 7 through 12
       11.786       0.6176      -7.9387       2.9775      -4.6945       1.9837
      -24.133       0.6558       12.523      -12.529        64.94      -57.444
       0.7988      -3.2023      -2.1548      -4.4796      -11.711       10.429
      -3.1711      -4.4393       8.2228       4.1663      -22.071       10.527
      -2.0555      -4.7131       3.3568      -3.0988      -10.928       3.2757
      -7.0154     -0.65847      -9.5715       4.1895     -0.08637    -0.082059
      -11.072       15.094      -1.6049       2.4602      -3.5524       15.743
       19.427      -157.24       6.7272      -2.4479      -62.317      -95.309
      -2.0436       6.4916      -40.388      -54.908       8.9926       8.5951
       7.2704      -2.4857      -58.468      -133.17      -10.124        23.79
     -0.17801        -2.88    -0.23971       3.3707      -30.128       18.726
       2.4619       1.1326      -2.5994       1.8672      -4.5338    -0.46137
       14.973      -0.7045      -10.723       1.7123      -11.546       8.0469
      -2.5149      -2.6621      0.48272       -5.357      -6.2492       6.0157
       -23.79       2.3553       18.571      -16.999       48.496      -45.132
      -42.912      -8.5545       27.618       1.6847       58.471      -33.137
   0.0086051     0.000831    0.0046559     0.001084    -0.14781    -0.29191
     0.01651    0.0020796   -0.0072498    0.0026513    -0.13127      -0.1058
  Columns 13 through 18
      -2.017      -4.0649       5.0383       -4.419   0.0013585   -0.0072002
      -5.1132      -158.03      -120.28      -302.33    -0.29548     0.093927
      -18.445      -178.73      -9.8009      -1984.6    0.096414    -0.073816
      -10.168      -15.821       127.52        -28.4      0.1823     -0.56244
       2.0653       6.9923      -186.71      -914.68     0.13434       3.7166
     0.068663      0.55012      -6.5463      -10.415      3.0514    -0.014789
      -3.6411       8.1747      -64.386       9.9744     -1.5739     -0.86095
       15.399      -3.1988       1566.5       2887.6     -0.2454     -0.13979
       45.462      -8.1581      -230.97       2268.2     -1.7195      0.77527
       98.502      -5.8969      -343.55       5776.4     0.75819     -0.43547
      -4.9662      -7.7627      -1301.7      -2910.5    -0.55124     -0.11427
       7.1295       66.907      -2215.2      -1449.7     0.19517     -0.40374
      -19.283       -51.99      -293.92       9996.3   -0.037171      0.34085
      -14.468      -146.41      -12.604      -2290.8    0.097226    -0.050565
      -1.2107      -123.63      -563.11      -587.48     0.32486    -0.063468
       0.2529        8.579      -259.24      -6281.4      2.0286       1.2011
     -0.15937    0.0074415       4.7603      -3.9787           0            0
       0.3076    -0.042156       1.7448       21.073           0            0
  Columns 19 through 20
      -1.2459       -2.289
       3.2991       3.4041
      -2.8148        2.161
       1.3054      0.28736
      0.44748      -1.0733
    -0.096757     -0.20641
      0.57513      -3.3422
      0.11186     -0.11686
     -0.26979       2.1066
      0.17804      -1.2112
      0.24748     -0.55919
       -1.894       1.0141
      -2.3213      -2.0712
      -1.4476       1.9367
        8.288     -0.37388
      -15.347       26.283
            0            0
            0            0
```

Fig. A2 Lateral–directional control law for case 1.

Figs. A1 and A2, respectively. These data are the outputs displayed on the MATLAB command window. For the state-space data for other cases, contact the first author.

References

[1]Doyle, J. C., "Analysis of Feedback System with Structured Uncertainties," *IEE Proceedings, Part D*, Vol. 129, No. 6, 1982, pp. 242–250.

[2]Safonov, M. G., "Stability Margins of Diagonally Perturbed Multivariable Feedback Systems," *IEE Proceedings, Part D*, Vol. 129, No. 6, 1982, pp. 251–256.

[3]Doyle, J. C., Wall, J. E., and Stein, G., "Performance and Robustness Analysis for Structured Uncertainty," *Proceedings of the 21st IEEE Conference on Decision and Control*, IEEE Publications, Piscataway, NJ, 1982, pp. 629–636.

[4]Tits, A. L., and Fan, M. K. H., "On the Small-μ Theorem," *Automatica*, Vol. 31, No. 8, 1995, pp. 1199–1201.

[5]Balas, G. J., Doyle, J. C., Glover, K., Packard, A., and Smith, R., *μ-Analysis and Synthesis Toolbox*, MUSYN, Inc., Minneapolis, MN, and The MathWorks, Inc., Natick, MA, 1995, pp. 4-1–4-84.

[6]Khatri, S., and Parrilo, P. A., "Spherical μ," *Proceedings of the 1998 American Control Conference*, IEEE Publications, Piscataway, NJ, 1998, pp. 2314–2318.

[7]Parrilo, P. A., and Khatri, S., "On Cone-Invariant Linear Matrix Inequalities," *IEEE Transactions on Automatic Control*, Vol. 45, No. 8, 2000, pp. 1558–1563.

[8]Fan, M. K. H., Tits, A. L., and Doyle, J. C., "Robustness in the Presence of Mixed Parametric Uncertainty and Unmodeled Dynamics," *IEEE Transactions on Automatic Control*, Vol. 36, No. 1, 1991, pp. 25–38.

[9]El Ghaoui, L., Carrier, A., and Bryson, A. E., Jr., "Linear Quadratic Minimax Controllers," *Journal of Guidance, Control, and Dynamics*, Vol. 15, No. 4, 1992, pp. 953–961.

[10]El Ghaoui, L., "Fast Computation of the Largest Stability Radius for a Two-Parameter Linear System," *IEEE Transactions on Automatic Control*, Vol. 37, No. 7, 1992, pp. 1033–1037.

[11]Morton, B. G., "New Applications of Mu to Real-Parameter Variation Problems," *Proceedings of the 24th IEEE Conference on Decision and Control*, IEEE Publications, Piscataway, NJ, 1985, pp. 233–238.

[12]Dailey, R. L., and Gangsaas, D., "Worst-Case Analysis of Flight Control Systems Using the Structured Singular Value," AIAA Paper 89-2018, July 1989.

[13]Wise, K. A., Mears, B. C., Tang, C.-K., and Godhwani, A., "Convex Hull Program Evaluating Control System Robustness to Real Parameter Variations," AIAA Paper 90-3339, Aug. 1990.

[14]Ferreres, G., and M'Saad, M., "Parametric Robustness Evaluation of a H_∞ Missile Autopilot," *Journal of Guidance, Control, and Dynamics*, Vol. 19, No. 3, 1996, pp. 621–627.

[15]Miotto, P., and Paduano, J. D., "Application of Real Structured Singular Values to Flight Control Law Validation," *Journal of Guidance, Control, and Dynamics*, Vol. 19, No. 6, 1996, pp. 1239–1245.

[16]Shin, J.-Y., Balas, G. J., and Packard, A. K., "Worst-Case Analysis of the X-38 Crew Return Vehicle Flight Control System," *Journal of Guidance, Control, and Dynamics*, Vol. 24, No. 2, 2001, pp. 261–269.

[17]Balakrishnan, V., Feron, E., Boyd, S., and El Ghaoui, L., "Computing Bounds for the Structured Singular Value via an Interior Point Algorithm," *Proceedings of the 1992 American Control Conference*, IEEE Publications, Piscataway, NJ, 1992, pp. 2195, 2196.

[18]Boyd, S., El Ghaoui, L., Feron, E., and Balakrishnan, V., *Linear Matrix Inequalities in System and Control Theory*, Vol. 15, Studies in Applied Mathematics, Society for Industrial and Applied Mathematics, Philadelphia, 1994, pp. 14–18.

[19]Gahinet, P., Nemirovski, A., Laub, A. J., and Chiali, M., *LMI Control Toolbox*, The MathWorks, Inc., Natick, MA, 1995, pp. 8-1–8-36.

[20]Feron, E., "A More Reliable Robust Stability Indicator for Linear Systems Subject to Parametric Uncertainties," *IEEE Transactions on Automatic Control*, Vol. 42, No. 9, 1997, pp. 1326–1330.

[21]Fu, M., and Barabanov, N. E., "Improved Upper Bounds of the Structured Singular Value," *Proceedings of the 34th IEEE Conference on Decision and Control*, IEEE Publications, Piscataway, NJ, 1995, pp. 3115–3120.

[22]Meinsma, G., Shrivastava, Y., and Fu, M., "Some Properties of an Upper Bound for μ," *IEEE Transactions on Automatic Control*, Vol. 41, No. 9, 1996, pp. 1326–1330.

[23]Stevens, B. L., and Lewis, F. L., *Aircraft Control and Simulation*, Wiley, New York, 1992, pp. 103–109.

[24]Terui, F., Tsukamoto, T., and Kajiwara, H., "LPV Controller Design for the Lateral–Directional Motion of Reentry Vehicle," AIAA Paper 99-4138, Aug. 1999.

[25]Apkarian, P., Gahinet, P., and Becker, G., "Self-Scheduled $\mathcal{H}_\infty$ Control of Linear Parameter-Varying Systems: A Design Example," *Automatica*, Vol. 31, No. 9, 1995, pp. 1251–1261.

[26]Stengel, R. F., and Ray, L. R., "Stochastic Robustness of Linear Time-Invariant Control Systems," *IEEE Transactions on Automatic Control*, Vol. 36, No. 1, 1991, pp. 82–87.

[27]Ray, L. R., and Stengel, R. F., "A Monte Carlo Approach to the Analysis of Control System Robustness," *Automatica*, Vol. 29, No. 1, 1993, pp. 229–236.